Modeling the Structural Effects of Rust in Concrete Cover

Ioannis Balafas[1] and Chris J. Burgoyne[2]

Abstract: Vast governmental budgets are spent annually to face corrosion problems of steel reinforcement in concrete bridges attributable to the extensive use of deicing salts. Corrosion controls the lifetime of a bridge, which has two distinct periods. During the first period, chlorides diffuse through the cover. When sufficient chlorides are formed at the rebars, corrosion initiates. This marks the start of the second period, during which rust with higher volume to bare steel is produced. The rust puts pressure on the cover, which finally leads to cover spalling. In this paper, a model is developed to determine the time span of the second period. The model includes a volume compatibility condition that allows for the proper introduction of compaction of all materials that contribute to cover spalling, including the rust. A new condition for marking failure of the cover is also established, based on fracture mechanics and strain energies. Finally, a new formula is proposed for the rate of rust production, which allows for the constant rust production at early and nonlinear diffusion dependant rates at latter stages of corrosion. **DOI: 10.1061/(ASCE)EM.1943-7889.0000215.**

CE Database subject headings: Corrosion; Cracking; Pressure; Concrete.

Author keywords: Corrosion; Cover cracking; Pressure; Rust.

Introduction

Extensive use of deicing salts on bridges leads to corrosion of steel reinforcement in concrete. In the United States, 15 million tons of deicing salts are used each year and 4–5 million tons are used in Canada (Wegner and Yaggi 2001). Alternatives to salt exist, but their cost is very high and their environmental effects have not been fully evaluated.

Corrosion problems in concrete have led researchers to investigate the viability of new corrosion-free reinforcement, such as fiber-reinforced polymer (FRP) bars. Those bars are expensive, but if long-term costs are taken into account, the economic picture changes dramatically (Balafas 2003; Burgoyne 2004).

It is not reasonable to expect all forms of construction to change because some concrete bridges have corrosion problems, so tools are needed to identify which structures are likely to have problems. Sensible whole-life costing procedures can then be applied to those structures, so that informed decisions can be made at the time that the structure is procured.

Corrosion is clearly a function of the environment to which the structure is exposed. The lifetime of a bridge that is exposed to chlorides has two distinct periods (Tuutti 1980; Uomoto and Mirsa 1988). During the first period, chlorides penetrate to the bar depth until the bar starts to corrode. The corrosion products of steel have a greater volume than the metal, and as a result, a pressure is exerted on the cover, which eventually leads to spalling. This paper covers this second period of time, when the rust is generating enough pressure to crack the cover.

This paper is part of a larger study to investigate the effect of the environment on the time needed for structures to become unserviceable because of corrosion. The first paper considers how the environment affects the time needed for chlorides to reach the concrete (Balafas and Burgoyne 2009). This paper explains how the time needed to crack the cover can be related to the rate of rust production, whereas a third paper studies how the environment affects that rate of rust production (Balafas and Burgoyne 2009). Because of the scarcity of models that predict the lifespan as a function of environmental exposure, the work of these papers is combined to predict the environmental conditions when a structure's lifetime may be affected sufficiently by corrosion to justify the use of relatively expensive FRP reinforcement (I. Balafas and C. J. Burgoyne, "Initial Cost of Beams Reinforced and Prestressed with Fibre Reinforced Polymer Reinforcement," to be submitted to *Journal of Composites for Construction*).

The model presented here includes a volume compatibility condition that allows for the proper introduction of compaction of all materials that contribute to cover spalling, including the rust. Recent results shows that rust deforms substantially under compression (Konopka 2005). When rust compaction is properly included, the space needed for its accommodation reduces, with a corresponding reduction in the exerted pressure on the cover.

A new condition for marking failure of the cover is also established, based on fracture mechanics and strain energies. Finally, a new formula is proposed for the rate of rust production. The formula is based on Faraday's law and on work by Liu and Weyers (1998a). Results show good agreement with existing experimental data on specimens under uniform corrosion.

Time to Cracking Model

After corrosion initiation, hydrated rust accumulates around the bar, causing pressure and leading to cover cracking. The ability to predict the time to cover cracking is important because it marks the end of structure's fully effective service life.

To predict the damage caused by corroding reinforcing bars, knowledge of the state of stress in the surrounding concrete is required, and this can be determined by means of a concrete ring

[1]Dept. of Civil and Environmental Engineering, Univ. of Cyprus, PO Box 20537, 1678 Nicosia, Cyprus. E-mail: ibalafas@ucy.ac.cy

[2]Dept. of Engineering, Univ. of Cambridge, Trumpington St., Cambridge, CB2 1PZ, UK. E-mail: cjb@eng.cam.ac.uk

Note. This manuscript was submitted on July 16, 2009; approved on August 23, 2010; published online on August 27, 2010. Discussion period open until August 1, 2011; separate discussions must be submitted for individual papers. This paper is part of the ***Journal of Engineering Mechanics***, Vol. 137, No. 3, March 1, 2011. ©ASCE, ISSN 0733-9399/2011/3-175–185/$25.00.

model (Fig. 1). The radial stresses on the concrete resulting from the volume increase of hydrated red rust, can be regarded as a uniform pressure acting on a thick-walled concrete ring, whose thickness is determined from the thinnest concrete cover around the bar, giving the shortest crack path from the bar to the free surface. The concrete ring approximates the effect of surrounding concrete, but due to different geometry between the cover ring model and the real cover, the stresses will only approximately correspond to the stresses in the real situation. However, the stresses are likely to be reasonable where the cover is thinnest, which is likely to be the critical section, so the concrete ring model can be accepted for the analysis (Tepfers 1979; Bažant 1979a; Martin-Perez et al. 2000).

Background

Previous attempts to model the presence of rust in concrete cover can be found.

Bažant (1979b) was the first to consider the problem. He used thick-wall cylinder formulas to evaluate stresses generated by the rust, but he assumed that the cover fails with the first appearance of a crack on the inner surface of the cylinder.

Molina et al. (1993) used finite elements to model cover cracking. It was a good early modeling attempt, but it made a number of simplifying assumptions. Rust production was assumed to be constant, whereas the long-term properties of concrete were not taken into account and compaction of the rust was not properly introduced.

Liu and Weyers (1998a) performed experiments on concrete slabs and used thick-wall theory for elastic and partially cracked cover to model cover cracking. They proposed a formula for rust production that takes into account the reduction in rust production rate as the rust layer thickens. The phenomenon is well known (Melchers 2003b; Melchers and Jeffrey 2005), but their formula has not yet been proven through experimentation. Additionally, Liu and Weyers' model formulation does not take into account rust compaction and crack space for rust filling.

Martin-Perez (1999) extends the thick wall formula, but does not study the cracked part of concrete in detail. He introduced compatibility conditions but did not properly model rust compaction, and the model gives short times-to-cover cracking. Pantazopoulou and Papoulia (2001) then introduced the Liu and Weyers formula for rust production and focused on detailed modeling of cracked concrete. They introduced concrete softening and allowed for the crack presence, which gave space where the rust could be accommodated; the result was reduced pressure on the cover and increased time to failure. They analyzed the behavior of the cover using finite differences. Other models appear at a later stage

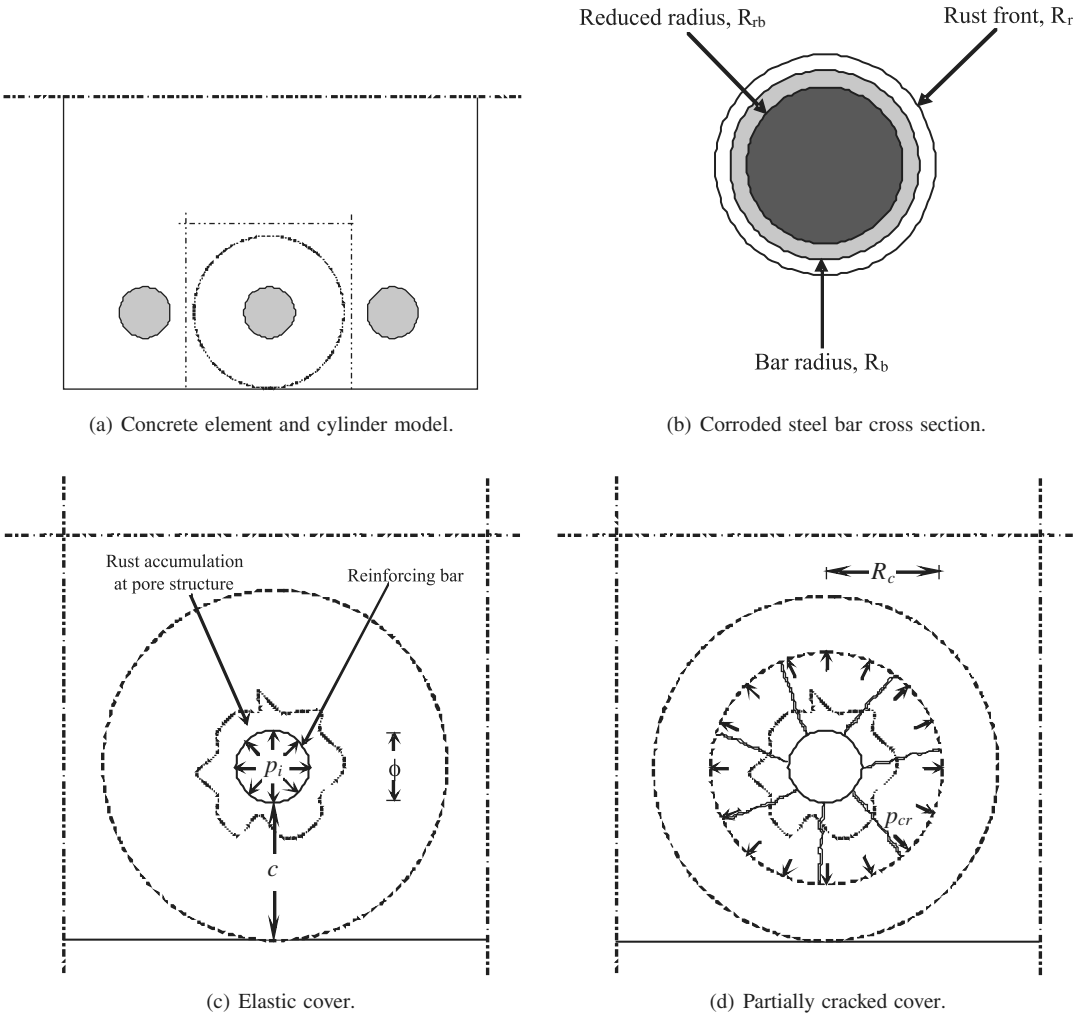

(a) Concrete element and cylinder model.

(b) Corroded steel bar cross section.

(c) Elastic cover.

(d) Partially cracked cover.

Fig. 1. Idealization of cover concrete as a thick-walled cylinder: (a) concrete element and cylinder model; (b) corroded steel bar cross section; (c) elastic cover; (d) partially cracked cover

following similar lines (Pantazopoulou and Papoulia 2001) using thick-wall cylinder formulas (Bhargava et al. 2006; Maaddaay and Soudki 2007; Zhao 2006).

Finally, fracture mechanics have been implemented to model cover cracking (Ohtsu and Yosimura 1997; Williamson and Clark 2000). The intention of those models is not to give good time predictions but to enhance understanding on crack initiation and propagation inside the cover.

Recently Achinta and Burgoyne (2008) used fracture mechanics concepts, based on strain energies [first introduced by Hutchinson and Suo (1992)], to model crack propagation in concrete beams strengthened with FRP plates. In the early stages of rusting, several cracks form in the concrete cover, but at failure, only one propagates unstably to the surface (Ohtsu and Yosimura 1997).

The model presented here uses thick-wall cylinder theory to solve for stresses but fracture concepts to determine failure. Rust production rates are modified according to recent corrosion test data, and since the process is slow, allowance is made for the long-term properties of concrete.

Rust Properties

The properties of rust are not well known, although recent work has indicated that rust properties differ significantly from those used by current cover-cracking models (Konopka 2005; Suda et al. 1993). The values found in Konopka (2005) are used here.

Konopka obtained rust samples from iron filings produced from a steel reinforcing bar. The process was accelerated by bubbling air through water containing a mild acid while impressing an electrical current. The resulting rust flakes were dried with as little handling as possible and then tested in small versions of standard soil mechanics triaxial and oedometer cells. The range of values measured for the elastic modulus was in the range 40–87 MPa, and 0.48–0.54 GPa for the bulk modulus.

Rust production rate is assumed to follow a rule that combines two earlier predictions. It is postulated that the rate of production for low rust thicknesses is linear and follows Faraday's law, but when the rust thickness increases the rate reduces, as ions have to diffuse through an increasing rust thickness for rust production to proceed. This phenomenon is introduced by considering a formula proposed by Liu and Weyers (1998a). That formula gives unrealistic corrosion rates at the start of corrosion, hence the introduction of the combined rule (Balafas and Burgoyne 2009).

Recent tests on rust layers have revealed that the inner layers are denser than outer layers (Melchers 2003a). To include the preceding, the following formula is included (Balafas and Burgoyne 2009):

$$\frac{dM_r}{dt} = \frac{k_p}{M_r^{n_l}} \Rightarrow M_r = \left(n_l \int k_p dt\right)^{1/n_l} \text{ (kg/m)} \tag{1}$$

The coefficient $n_l = 2$ for rust with uniform density across the thickness but increases towards 3 as the nonlinearity of the rust production versus time increases. Values for k_p are dependent on n_l; they decrease while n_l increases from 2 to 3. Values of k_p were back-calculated to reach agreement with published experimental data. A detailed description of the aforementioned modifications, as included in the current model, can be found in (Balafas and Burgoyne 2009).

Pressure on Cover

To analyze the effects of the rust products on the cover, a concrete ring around the bar is assumed (Bažant 1979a; Liu and Weyers 1998b). The thickness of the ring is equal to the minimum concrete cover, since this is where the critical crack is expected to form. Fig. 1(a) shows the bottom of a beam reinforced with three tensile bars; the concrete ring around the middle bar is highlighted. The bar is assumed to corrode uniformly along its length, so only a 2D plane strain analysis is performed.

When corrosion initiates, the original radius of the bar R_b reduces to R_{rb}; but because the rust possesses higher volume than the original metal, the effective radius of the bar increases to R_r [Fig. 1(b)], causing pressure on the cover. Initially, however, the rust products fill pores in the concrete around the bar, so no pressure is exerted until the pores have filled (Liu 1996; Martin-Perez 1999; Pantazopoulou and Papoulia 2001; Bhargava et al. 2006) [Fig. 1(c)]. The cover is elastic until the stress at the steel-concrete interface reaches the concrete's tensile strength; cracks then propagate and stop where the stress at the tip of the crack can be sustained by the concrete. In this partially cracked state (Martin-Perez 1999), there are thus two parts to the cover: a cracked cover and an elastic cover [Fig. 1(d)].

Fig. 2 shows a radial slice from the center of the bar (on the left) to the surface of the concrete for three different stages of the analysis. The nomenclature used in the analysis is shown in the figure.

Elastic Concrete Ring

The mass of rust formed is given from

$$M_r = \frac{1}{r} M_s \text{ (kg/m)} \tag{2}$$

in which M_r and M_s are the mass of rust and consumed steel, respectively.

The corresponding volumes of steel consumed are thus

$$V_r = \frac{M_r}{\rho_r} \text{ (m}^3\text{/m)} \tag{3}$$

$$V_s = \frac{M_s}{\rho_s} \text{ (m}^3\text{/m)} \tag{4}$$

where ρ_s and ρ_r = density of steel ($7,850$ kg/m^3) and rust ($4,115$ kg/m^3) (Balafas and Burgoyne 2009), respectively.

Because some of the iron has been consumed, the steel radius, R_{rb}, reduces to

$$R_{rb} = \sqrt{R_b^2 - \frac{V_{cs}}{\pi}} \text{ (m)} \tag{5}$$

where V_{cs} = the steel volume consumed and R_b = the original bar radius. The total bar radius, R_r, including rust, will be greater than R_b

$$R_r = R_{rb} + t_r \text{ (m)} \tag{6}$$

in which t_r = the oxide layer thickness that builds up around the bar. The volume of oxide generated, V_r, is

$$V_r = \pi(R_r^2 - R_{rb}^2) \text{ (m}^3\text{/m)} \tag{7}$$

By substituting Eq. (6) into Eq. (7) and rearranging,

$$V_r = \pi t_r(2R_{rb} + t_r) \text{ (m}^3\text{/m)} \tag{8}$$

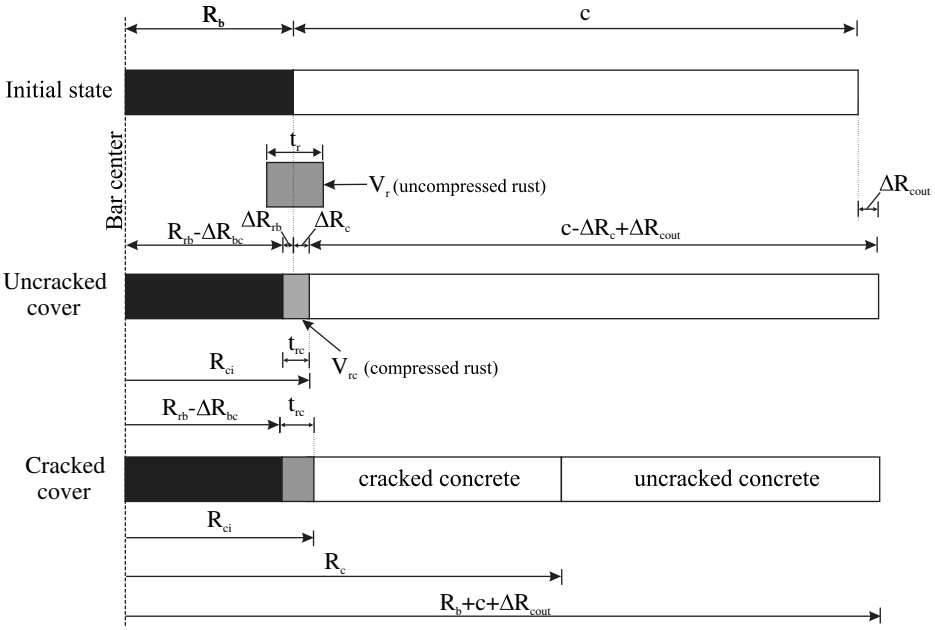

Fig. 2. Half cover plus bar slice with dimensions

which can finally be solved for t_r as

$$t_r = \sqrt{R_{rb}^2 + \frac{V_r}{\pi}} - R_{rb} \text{ (m)} \tag{9}$$

Part of the rust formed by corrosion fills the pores that surround the bar (Liu and Weyers 1998b), whereas the rest causes pressure on the concrete [Figs. 1(c) and 1(d)]. The rust that fills pores is taken into account by an equivalent rust thickness t_f, which, according to tests by Liu and Weyer (1998), is between 10 and 100 μm thick. This thickness is a strong function of concrete porosity and environmental exposure, and more tests are needed to determine those relationships. To include that process t_r is set to zero when $t_r \leq t_f$. When $t_r > t_f$,

$$t_r = \sqrt{R_{rb}^2 + \frac{V_r}{\pi}} - R_{rb} - t_f \text{ (m)} \tag{10}$$

t_f can be estimated if the thickness of the porous zone to be filled with rust t_p, and the concrete porosity V_p, are known. Equating the volumes of consumed rust to fill the porous zone to the available volume of pores

$$t_f = \frac{(R_b + t_p)V_p}{R_b} \text{ (m)} \tag{11}$$

Because of the presence of rust, the effective bar radius will increase by

$$\Delta R_b = R_b - R_{rb} + t_r \text{ (m)} \tag{12}$$

The pressure that acts on the cover because of the rust presence can be found by equating the change of volume of steel ΔV_s and concrete ΔV_c to that of the amount of rust that is under compression V_{rc}

$$\Delta V_s + \Delta V_c = V_{rc} \text{ (m}^3\text{/m)} \tag{13}$$

The volume change of steel is a function of the direct steel volume reduction attributable to rust production and compression attributable to the rust pressure on its surface. It can be given from

$$\Delta V_s = 2\pi\left(R_b - \frac{\Delta R_{rb}}{2}\right)\Delta R_{rb} \text{ (m}^3\text{/m)} \tag{14}$$

where ΔR_{rb} = the radius change in the sound steel caused by rust production and pressure (compression positive)

$$\Delta R_{rb} = R_b - R_{rb} + \Delta R_{bc} \text{ (m)} \tag{15}$$

ΔR_{bc} = the change in the sound steel radius caused by pressure only; assuming that steel is linearly elastic solid cylinder under external pressure, ΔR_{bc} is given by (Timoshenko 1956)

$$\Delta R_{bc} = \frac{pR_{rb}}{E_s}(1 - \nu_s) \text{ (m)} \tag{16}$$

In Eq. (13), V_r = the rust volume that actually exerts the pressure, but the rust itself will be under pressure inside the cover. The uncompressed rust volume is

$$V_r = 2\pi\left(R_{rb} + \frac{t_r}{2}\right)t_r \text{ (m}^3\text{/m)} \tag{17}$$

The rust's volumetric strain, ϵ_r, under pressure p is

$$\epsilon_{Vr} = \frac{p}{K_r} \tag{18}$$

where K_r = rust's bulk modulus.

The volume of rust is then compressed to

$$V_{rc} = V_r(1 - \epsilon_r) \text{ (m}^3\text{/m)} \tag{19}$$

which reduces the thickness of the rust from t_r to t_{rc} attributable to compression. t_{rc} can be determined by setting V_r and t_r to V_{rc} and t_{rc}, respectively, in Eq. (17), and solving for t_{rc}

$$t_{rc}^2\pi + t_{rc}2\pi - V_{rc} = 0 \tag{20}$$

where the value for the positive root of the polynomial = t_{rc}.

The increase of the internal radius of the concrete ring ΔR_c, attributable to the volume change of the concrete ring cover, can be determined in a closed form by the classical analysis of a thick-walled cylinder (Timoshenko 1956)

$$\Delta R_c = \frac{p_c(R_b + t_{rc})}{E_{ct}} \left[\frac{(c + R_b)^2 + R_{ci}^2}{(c + R_b)^2 - R_{ci}^2} + \nu_c \right] \text{ (m)} \quad (21)$$

where c = the cover depth and E_{ct} = the elastic modulus of concrete at time t and its evaluation is according to CEB (1993). E_{ct} reduces with time to allow for long-term concrete properties, i.e., creep and shrinkage. The pressure on the concrete cover is reduced from p to p_c

$$p_c = p \frac{R_{rb}}{R_{ci}} \text{ (N/m}^2\text{)} \quad (22)$$

so the concrete volume change is

$$\Delta V_c = 2\pi \left(R_{ci} + \frac{\Delta R_c}{2} \right) \Delta R_c \text{ (m}^3\text{/m)} \quad (23)$$

The pressure exerted on the concrete by the rust products can be determined by substituting Eqs. (14), (17), and (23) into Eq. (13) and solving for p.

Partially Cracked Ring Model

When a crack initiates at the interface between bar and concrete, it will fully propagate through the cover only when the tensile concrete capacity of the ring is exhausted. Thus, the concrete will be cracked at places where the tangential stresses have exceeded f_t and uncracked in the outer part of the cylinder where the stress is less than f_t. The inner part of the cover can be envisaged as a series of teeth that project inward from the uncracked cover to the steel surface [Fig. 1(d)]. The internal pressure at the rust/concrete interface acts radially through these teeth, but the tangential stresses now show softening behavior.

After crack propagation, the inner radius of the uncracked ring is lower than before, with a corresponding reduction in pressure (Wang and Liu 2004)

$$p_{cr} = \frac{pR_{rb} - \int_{R_{ci}}^{R_c} \sigma_t(R) dR}{R_c} \text{ (N/m}^2\text{)} \quad (24)$$

R_c = the radius at the crack front and $\sigma_t(R)$ = the tangential stress of cracked concrete at radius R from the bar's center. $\sigma_t(R)$ will be on the softening branch of concrete's tensile stress-strain curve. The concrete is assumed to be linear-elastic up to its tensile strength f_t, whereas the softening curve is bilinear: the first part f_t-$0.15f_t$ is steeper than the second $0.15f_t$-0 (Pantazopoulou and Papoulia 2001; Wang and Liu 2004)

$$\sigma_t(R) = \begin{cases} E_{ct}\epsilon_t(R) & \text{for } \epsilon_t(R) \le \epsilon_{ct} \\ f_t \left[1 - 0.85 \frac{\epsilon_t(R) - \epsilon_{ct}}{\epsilon_1 - \epsilon_{ct}} \right] & \text{for } \epsilon_{ct} < \epsilon_t(R) \le \epsilon_1 \\ 0.15 f_t \frac{\epsilon_u - \epsilon_t(R)}{\epsilon_u - \epsilon_1} & \text{for } \epsilon_1 < \epsilon_t(R) \le \epsilon_u \end{cases} \quad (25)$$

ϵ_{ct} = the strain at f_t, ϵ_1 = the strain at $0.15f_t$, and ϵ_u = the strain at the end of the second softening branch.

The tangential strain at radius R in the cracked concrete $\epsilon_t(R)$ is determined by assuming linear strain distribution across the thickness of the cracked cover, i.e., between the strain at the rust-concrete interface $\epsilon_t(R_{ci})$ and the strain at the crack front (R_c) $\epsilon_t(R_c)$

$$\epsilon_t(R) = \epsilon_t(R_{ci}) - \frac{\epsilon_t(R_{ci}) - \epsilon_t(R_c)}{R_c - R_{ci}} (R - R_{ci}) \quad (26)$$

where $\epsilon_t(R_c)$ can be expressed as

$$\epsilon_t(R_c) = \frac{\Delta R_c}{R_c} \quad (27)$$

the concrete ring displacement, at crack front (R_c), ΔR_c can be found from (Timoshenko 1956)

$$\Delta R_c = p_{cr} \frac{R_c}{E_{ct}} \left[\frac{(c + R_b)^2 + R_c^2}{(c + R_b)^2 - R_c^2} + \nu_c \right] \text{ (m)} \quad (28)$$

ν_c is the Poisson ratio of concrete.

On the other hand, the strain at the rust-concrete interface $\epsilon_t(R_{ci})$ in Eq. (26) is equal to

$$\epsilon_t(R_{ci}) = \frac{\Delta R_{ci}}{R_{ci}} \quad (29)$$

where the concrete ring displacement at the rust-concrete interface ΔR_{ci} is given from

$$\Delta R_{ci} = \Delta R_c + \Delta R_{cr} \text{ (m)} \quad (30)$$

ΔR_{cr} = cracked concrete compressive displacement, which is found by assuming that concrete is under uniaxial compression as follows:

$$\Delta R_{cr} = \frac{(p_c + p_{cr})}{2E_{ct}} (R_c - R_b) \text{ (m)} \quad (31)$$

Hence ΔV_c for cracked concrete is given from

$$\Delta V_c = 2\pi \left(R_c + \frac{\Delta R_{ci}}{2} \right) \Delta R_{ci} + V_{cr} \text{ (m}^3\text{/m)} \quad (32)$$

V_{cr} = the change of concrete volume attributable to cracks; while cracks are opening, some of the rust will be consumed to fill them and most will not cause pressure on concrete. To model the cracked part of the cylinder, smeared cracking is assumed and average stresses and strains are used in the calculations (Pantazopoulou and Papoulia 2001).

By assuming that the cracks will have their maximum widths at the rust front $R_b + \Delta R_{ci}$ and zero at the crack front R_c, the available total space between cracks can be approximated by

$$V_{cr} = \frac{1}{2} w[(R_c - (R_b + \Delta R_{ci})] \text{ (m}^3\text{/m)} \quad (33)$$

The total crack width openings along the rust front perimeter $R_b + \Delta R_{ci}$ [Fig. 1(b)], can be estimated from

$$w = \epsilon_t(R_{ci}) 2\pi (R_b + \Delta R_{ci}) \text{ (m)} \quad (34)$$

where $\epsilon_t(R_{ci})$ = the tangential strain at the rust front

$$\epsilon_t(R_{ci}) = \frac{\Delta R_{ci}}{R_b} \quad (35)$$

In summary: for partially cracked cover, only the change of concrete volume ΔV_c is modified, in comparison to elastic cover calculations ("Elastic Concrete Ring" section), so

- Eqs. (14) and (19) are used to determine the volume of rust and change of steel volume respectively,
- Eq. (32) is used instead of Eq. (23):

By substituting Eqs. (14), (19), and (32) into Eq. (13), p_{cr} can be determined.

The uncracked part of the ring can be treated as a thick-walled cylinder with an inner radius of R_c subjected to internal pressure p_{cr}, and from Eq. (24) the tangential stress at the outer part of the concrete ring is equal to

$$\sigma_t = p_{cr}\frac{R_c^2}{(R_{ci}+c)^2 - R_c^2}\left(1 + \frac{(R_{ci}+c)^2}{R^2}\right) \text{ (N/m}^2\text{)} \quad (36)$$

in which R takes values from $R_c \le R \le R_{ci} + c$.

To find the depth of the crack front, R_c, σ_t is set equal to f_t, R equal to R_c, and Eq. (36) is rearranged in powers of R_c as

$$f_t R_c^3 + R_{ci} p R_c^2 - (c + R_{ci})^2 f_t R_c + (c + R_{ci})^2 R_{ci} p = 0 \quad (37)$$

from which the root $R_{ci} \le R_c \le R_{ci} + c$ is chosen for the crack front.

Cover Failure

As pressure increases, cracks propagate through the cover. Experimental results have shown that, although at the early stages of crack propagation several cracks appear, by the end of the test there is a single crack that finally breaks the cover (Nguyen et al. 2006; Ohtsu and Yosimura 1997) on the weakest side of the concrete element. When this crack appears, the internal stresses relax, which stops the propagation of other internal cracks (Nguyen et al. 2006). To determine when a crack propagates unstably through the cover, fracture-mechanics concepts are employed.

As existing cracks extend, the energy needed to form associated new surfaces depends on the interface fracture energy and must be compared with the energy released by the system, which in turn depends on the change of the strain energy stored in the system (Hutchinson and Suo 1992; Achinta and Burgoyne 2008). The amount of energy needed to form new surfaces is measured by the fracture energy density G_F.

Experiments have revealed that when a crack propagates unstably to the surface of the elements, the internal pressure is lost and the specimen has released all its strain energy (Torres-Acosta 1999).

The total elastic strain energy of the concrete ring consist of the elastic energy of:

- The elastic part of the cover concrete;
- The cracked part of the cover concrete;
- The compressed rust;
- The laterally compressed steel.

The tangential stresses through the elastic part of cover due to p_{cr} can be found from (Timoshenko 1956)

$$\sigma_t = p_{cr}\frac{R_c^2}{R^2}\left[\frac{(c+R_b)^2 + R^2}{(c+R_b)^2 - R_c^2}\right] \text{ (N/m}^2\text{)} \quad (38)$$

and the radial stresses from

$$\sigma_r = p_{cr}\frac{R_c^2}{R^2}\left[\frac{(c+R_b)^2 - R^2}{(c+R_b)^2 - R_c^2}\right] \text{ (N/m}^2\text{)} \quad (39)$$

where R = the radius and takes values between R_c and $(c + R_b)$.

The tangential and radial strains along the elastic cover due to p_{cr} may be expressed as

$$\epsilon_t = \frac{1}{E_c}(\sigma_t - \nu_c \sigma_r) \quad (40)$$

$$\epsilon_r = \frac{1}{E_c}(\sigma_r - \nu_c \sigma_t) \quad (41)$$

The short-term elastic modulus of concrete E_c is used, since it is the elastic energy that would be released on unloading that is of interest, whereas in the calculations of space available to accommodate the rust, the long-term modulus E_{ct} is used instead.

The total strain energy of the elastic ring cover concrete is

$$SE_e = 2\pi \int_{R_c}^{c+R_b} (\sigma_t \epsilon_t + \sigma_r \epsilon_r) R dR \text{ (Nm/m)} \quad (42)$$

The evaluation of the tangential tensile stresses and the strains in the cracked part of the cover can be given from Eqs. (25) and (26), respectively, using concrete's short-term properties, i.e., E_c. Compressive radial stresses and strains in cracked concrete are found as follows:

$$\sigma_{rc} = \frac{1}{2}(p_{cr} + p_c) \text{ (N/m}^2\text{)} \quad (43)$$

$$\epsilon_{rc} = \frac{\sigma_{rc}}{E_c} \quad (44)$$

Hence, the total strain energy of cracked ring cover concrete per unit length is given by

$$SE_c = 2\pi \int_{R_{ci}}^{R_c} (\sigma_{tc} \epsilon_{tc} + \sigma_{rc} \epsilon_{rc}) R dR \text{ (Nm/m)} \quad (45)$$

The steel bar is under uniform $p_{i,\text{com}}$ compression, and the generated compressive tangential and radial stresses are constant over the bar

$$\sigma_{st} = \sigma_{sr} = p_c \text{ (N/m}^2\text{)} \quad (46)$$

whereas the tangential and radial strains are

$$\epsilon_{st} = \epsilon_{sr} = \frac{p_c}{E_s}(1 + \nu_s) \text{ (N/m}^2\text{)} \quad (47)$$

where ν_s = the Poisson's ratio of steel. The strain energy per unit length in the steel attributable to p_c is

$$SE_s = 2\pi \frac{p_c^2}{E_s}(1 + \nu_s) \int_0^{Rb} R dR \text{ (Nm/m)} \quad (48)$$

Konopka (2005) showed that on rust does not expand much once decompressed, which means that it contains very little elastic strain energy. It will be assumed to be negligible by comparison with the other components.

The total strain of the concrete ring per unit length attributable to the presence of rust is given by

$$SE_t = SE_e + SE_c + SE_s \text{ (Nm/m)} \quad (49)$$

Eq. (49) assumes a perfect bond between rebars and concrete.

The cover ring will fail when a crack propagates unstably along the weakest side toward the surface of the element. The energy release rate G_R is thus (Achinta and Burgoyne 2008)

$$G_R = \frac{\Delta SE_t}{n(R_b + c - R_c)} \text{ (Nm/m}^2\text{)} \quad (50)$$

where n = the number of cracks to break the cover. Normally $n = 1$. As previously mentioned, tests have shown that with the formation of the crack, pressure drops to zero, so ΔSE_t = effectively SE_t. The crack will extend to fail the cover only when the energy release rate G_R is greater than the fracture energy of concrete G_F; if not, there is insufficient energy for the flaw to propagate (Achinta and Burgoyne 2008) and the crack will continue to grow slowly. There is considerable work on the fracture energy of concrete, and published values lie between 0.080 to 0.154 N/mm

(Achintha 2009). The distance between the rebar and the surface of the concrete is too small for a fully developed fracture process zone to exist, so it is assumed that plastic energy dissipation is small and is hence neglected. The energy involved is effectively included in the measured values of fracture energy.

Model Evaluation

Experiments have been performed on the effect of corrosion on the cover (Liu and Weyers 1998b; Andrande et al. 1993). Times-to-cover cracking have been measured, as has the mass of rust needed to cause the cover to crack for prescribed corrosion rates i_{corr}. These experiments have been compared with the predictions of the current model, simulating the experimental conditions; the results are shown in Table 1, which shows that the model can give relatively close values for time-to-cover cracking and for the mass of rust needed. There is, however, a discrepancy between test and model predictions for specimen SA3.

Tests on cover cracking have also been published by Torres-Acosta (1999). The bars in his case were embedded in concrete cylinders with strength 53 N/mm^2 and cover depth range of 27–65 mm and were exposed to localized corrosion. The model of this work is built on the assumption of uniform corrosion. Tests have shown that maximum penetration depth under localized attack is about four to eight times that of uniform corrosion (González et al. 1995). The average experimental times-to-cover cracking were 3.5 times faster than this model's predictions. The average experimental depth of corrosion was six times that of model predictions.

Sketches of Torres-Acosta's failed specimens show that two or three cracks have penetrated the cover, but it is not clear whether they appeared at the same time. If so, the energy release rate, given by Eq. (50), has to be divided by the number of cracks that fail the cover, but this seems improbable. It is concluded, however, that the model presented here is only applicable for uniform corrosion.

Model Application

To illustrate how the model can be used, it is applied to an experiment performed by Liu and Weyers (1998a). Test Specimen SL1 shown on Table 2 is modeled.

Table 1. Analytical versus Experimental Results

Specimen	Parameter	Experiment	Model
Liu and Weyers (1998b)			
SL1	Time to cracking (years)	1.84	1.84
	Rust mass (kg/m^2)	0.393	0.405
SL2	Time to cracking (years)	3.54	3.65
	Rust mass (kg/m^2)	0.601	0.598
SL3	Time to cracking (years)	0.72	0.67
	Rust mass (kg/m^2)	0.298	0.228
SL4	Time to cracking (years)	2.38	2.87
	Rust mass (kg/m^2)	0.392	0.473
(Andrande et al. 1993)			
SA1	Time to cracking (days)	5	5.69
	Rust mass (mm)	0.016	0.016
SA2	Time to cracking (days)	4	2.84
	Rust mass (mm)	0.0128	0.0102
SA3	Time to cracking (days)	23	34.02
	Rust mass (mm)	0.00731	0.0106

Table 2. Input Parameters Used in the Analysis

Specimen	Bar diameter D_b [mm]	i_{corr} [$\mu A/cm^2$]	c [mm]	f_c [N/mm^2]
Liu and Weyers (1998b)				
SL1	16	2.41	48	31.5
SL2	16	1.79	70	31.5
SL3	16	3.75	27	31.5
SL4	12.7	1.80	52	31.5
(Andrande et al. 1993)				
SA1	16	100	30	30
SA3	16	100	20	30
SA4	16	10	20	30
Rust properties (Balafas and Burgoyne 2010)				
	r_m			0.643
	r_V			2.964
	r_d			1.907
	E_r (N/mm^2)			60
	K_r (kN/mm^2)			0.5
	n_l			2.00
	k_{coef}			0.086
	t_f (μm)			10
Concrete fracture				
	G_F (N/mm)			0.12

The analysis is executed by introducing a time counter. The produced rust is determined in each time step, which fills concrete pores and exerts pressure on cover. When the energy release rate G_R is greater than the fracture energy of concrete G_F, cover fails and analysis terminates.

Fig. 3 shows the reduction of steel rebar radius, as well as the increase of remaining steel plus rust radius. It shows that rebar radius losses of about 32 μm are enough to break the cover. At early stages, the rebar plus rust radius remains constant because the rust is consumed to fill the concrete pore structure around the bar. After less than 2 months, the pore structure is filled and new rust causes the bar plus rust radius to increase.

Fig. 4 show the crack propagation with time. Initially crack propagation is zero because rust is consumed to fill concrete pores and the space of the consumed steel. Cracks first appear at around

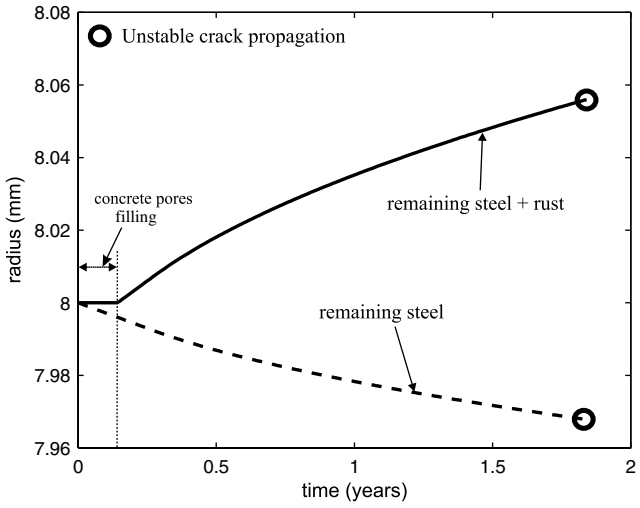

Fig. 3. Rebar radius with and without rust versus time

2 months. When cracks propagate, they create new space to accommodate rust whereas pressure as well as tensile concrete stresses drop at the crack tips, which arrest existing cracks. Once the newly formed space has been filled with rust, pressure picks up again and the cracks develop further.

The slope of the crack propagation decreases with time because the ring stiffness reduces, which allows higher deformations on the concrete ring, and hence, more space that can accommodate rust becomes available. The drop is enhanced because of the nonlinear rust production rate assumption [Eq. (1)]. Unstable crack propagation takes place when the cracked part of the cover reaches a radius of about 16.4 mm from the bar center, or 8.4 mm from the bar surface. Given that the cover depth is 48 mm, the cracked cover represents only 18% of total depth when failure occurs.

The evolution of pressure is shown in Fig. 5. The pressure drops, along with crack propagation, are also clearly visible; and the highest is at crack initiation. This coincides with the longest pause in crack propagation, as shown in Fig. 4. Pressures at two different depths are plotted: at the rust-concrete interface and at the crack front. The analysis has been conducted with and without tension stiffening effects, whereas ignoring them increases the pressure very slightly at the crack front.

Rates of volume changes for rust and sound rebar are shown in Fig. 6. The volume changes for the rebar include the change of volume attributable to steel consumption as well as those attributable to pressure. Rust has three times the volumetric strains of the rebar because of its low bulk modulus. The volumetric strain reductions, caused by drops of pressure, can be observed. They are not observed in the rebar's volumetric curve because the volume of steel consumed is large in comparison to volume changes caused by the pressure, as would be expected.

The preceding observation is confirmed through Fig. 7. The radius change at the rust-concrete interface, attributable to rust pressure, is approximately three times that of the outer ring radius, whereas the change in the rebar's radius attributable to the pressure change is almost insignificant.

Where rust is accommodated in the cover through time is shown in Fig. 8. It is highlighted that the steel volume decrease (mainly

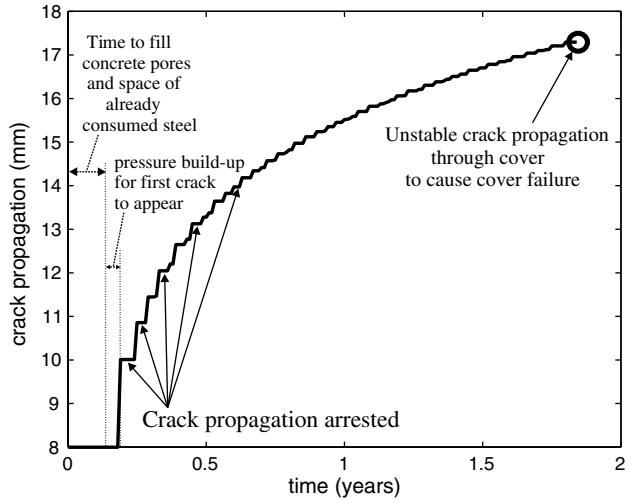

Fig. 4. Cover crack propagation versus time

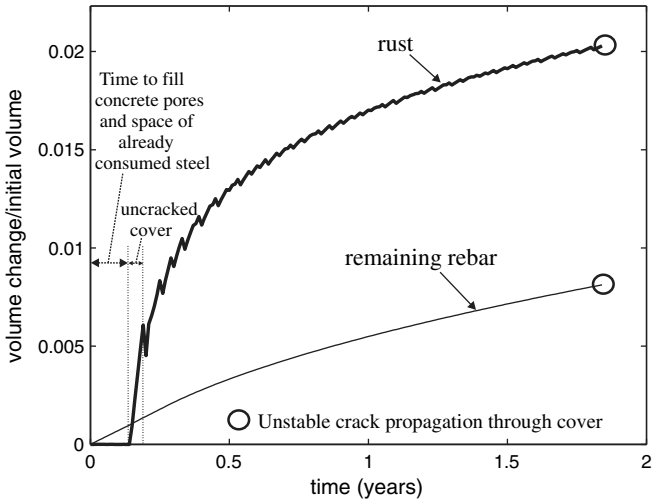

Fig. 6. Change of volume over initial volume for rust and rebar

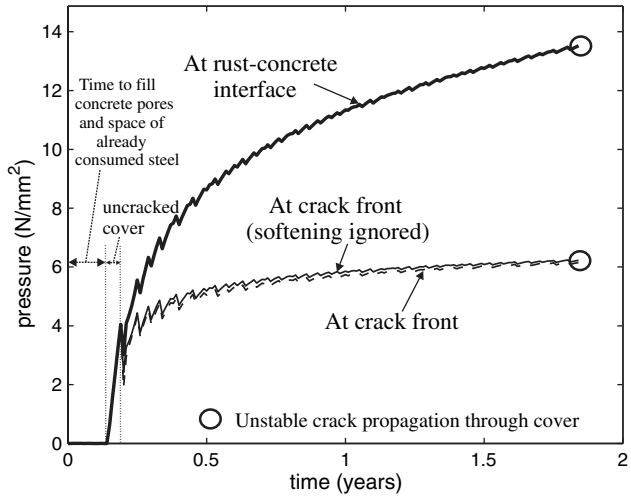

Fig. 5. Pressure buildup versus time at crack front and at rust-concrete interface with and without taking into account softening of concrete in tension

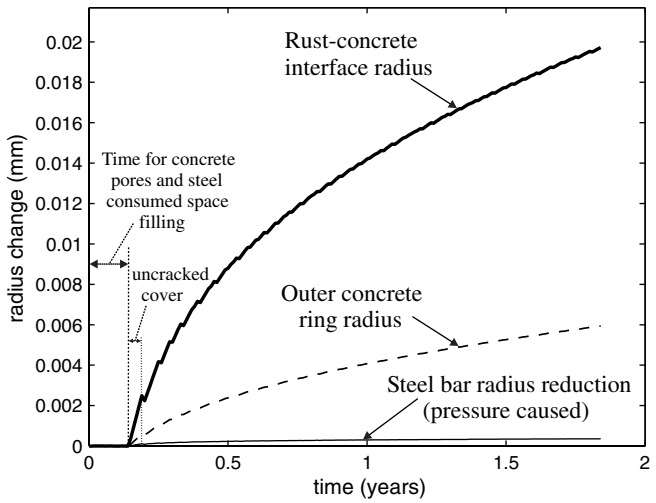

Fig. 7. Radius change of inner (rust-concrete interface) and outer concrete ring surfaces as well as steel bar radius reduction attributable to rust pressure only

because of steel consumption rather than steel contraction caused by pressure) and the inner concrete perimeter radial expansion are the two principal components of the total volume change. The volume formed attributable to cracks and radial compression of the cracked part of the cover represent only a small portion of the available total volume. Although Fig. 7 showed that the radius change for the inner concrete radius was more than double that of the outer, Fig. 8 shows that the volumes created by the expansions of those perimeters are comparable. During pore filling, the pressure is zero, so the total volume is equal to the steel consumption volume.

The mass of steel consumed and the mass of rust produced according to combined rules are plotted in Fig. 9, together with the corresponding masses if Faraday's law and Liu and Weyers' rule are also shown. The high steel consumption rates predicted by Liu and Weyers' rule occurred at a young age.

Fig. 10 shows the total energy buildup in the concrete ring. When total energy reaches the concrete's fracture energy, then a crack propagates unstably to break the cover. Pressure drops because crack propagations affect total ring energy, hence the highlighted energy drops highlighted on the figure. Total energy consists of strain energies from elastic concrete, cracked concrete, and steel bar [Eq. (49)]. Each contribution is shown in Fig. 11; the highest is from elastic concrete, whereas the lowest is from cracked concrete in tension (under softening). The cracked concrete possesses high energy for its small size, as shown in Fig. 4, because cracked concrete is under the highest pressure. Pressures reduce exponentially with cover depth. The evolutions of the tangential and radial part of the elastic cover with time are also shown in Fig. 11. The tangential stresses possess more than double the energy of the radial stress. The steel bar holds relatively high strain energy, despite the low deformations (Fig. 7) attributable to its high Young's modulus.

Finally, Fig. 12 illustrates the relationship between the energy release rate and pressure. At low pressures, the energy release rate pickup is low, but as the pressure increases and the cover cracks, it increases faster because of the reduction in the cover's stiffness. This gives increased deformations, adding to energy accumulation.

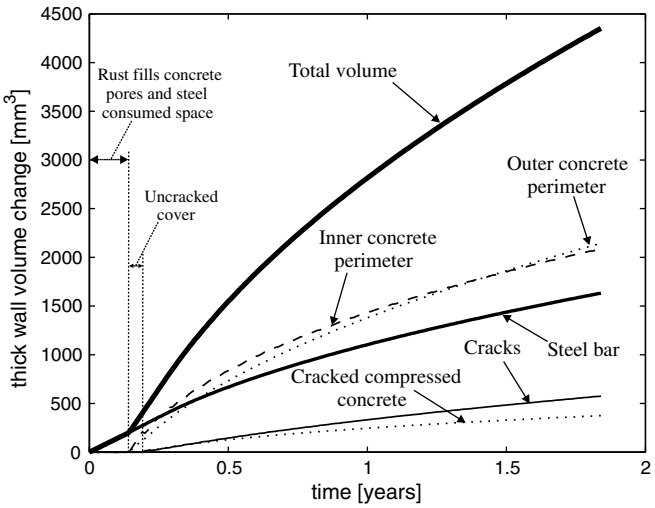

Fig. 8. Total volume created for rust accommodation in concrete cover and its components (per meter length) versus time

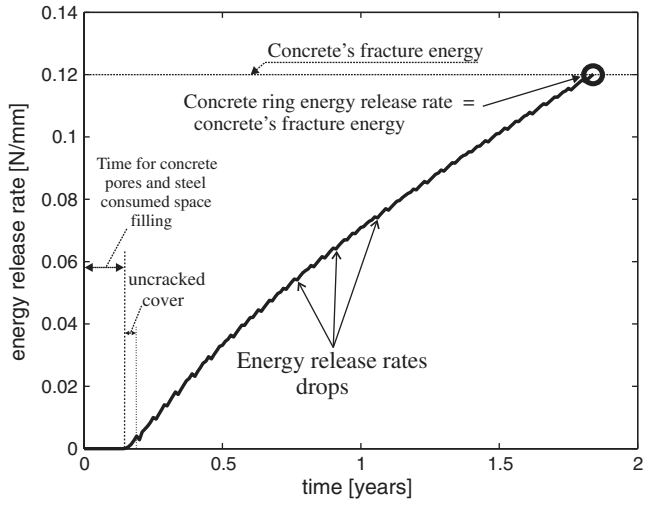

Fig. 10. Concrete ring energy release rate buildup (per meter length) versus time

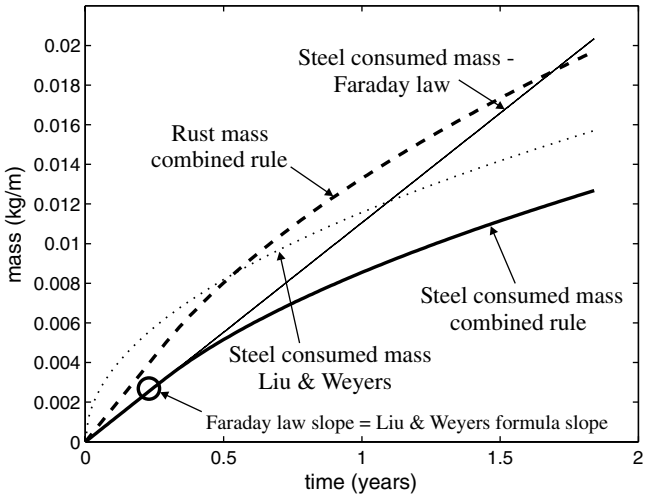

Fig. 9. Consumed steel and rust mass production versus time

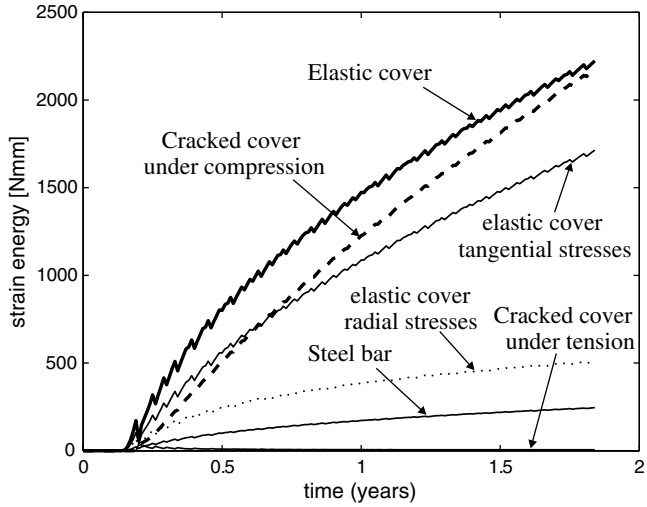

Fig. 11. Elastic concrete, cracked concrete, and steel bar strain energies, per meter length, versus time

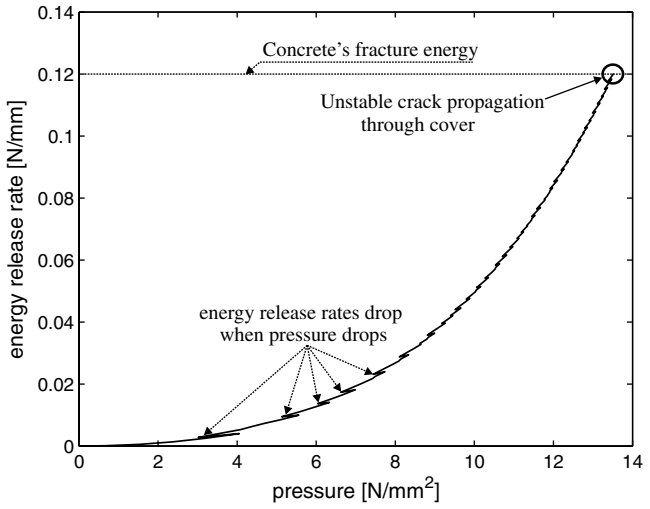

Fig. 12. Energy release rate (per meter length) buildup versus pressure

Conclusions

The model presented here determines the structural lifetime from initiation of corrosion to cover spalling. It is part of a bigger model (Balafas 2003), which was created to identify the conditions under which a bridge has a limited lifetime and fails to meet its intended design life. In these cases, new materials for concrete reinforcement like carbon, aramid, or glass are viable alternatives to steel.

The presented model assumes volume compatibility to determine the pressure caused by the rust products on the cover. It allows for the compaction of all materials affected by the pressure on the cover, including rust.

A fracture mechanics concept, based on the cover's strain energy has been introduced to identify cover failure. The rust properties assumed were based on experimental data on rust composition. A new rust production formula based on existing experimental evidence has also been introduced. The formula is a mixture of Faraday's law and a formula proposed by Liu and Weyers. The latter was modified to account for changes in rust layer diffusivity with thickening. Detailed concrete behavior has been introduced, including tension softening and the effect of creep, which is important since the pressure exerted by rust is a long-term loading.

Results show good agreement with existing data for specimens with bars under uniform corrosion. Results on specimens with bars with localized corrosion were considerably shorter than observed and more work is needed in this area.

Acknowledgments

The work was supported by the EU TMR Network "ConFibreCrete."

References

Achintha, P. M. M. (2009). "Fracture analysis of debonding mechanism for FRP plates." Ph.D. thesis, Engineering Dept., Univ. of Cambridge, Cambridge, UK.

Achintha, P. M. M., and Burgoyne, C. J. (2008). "Fracture mechanics of plate debonding." *J. Compos. Constr.*, 12(4), 396–404.

Andrande, C., Alonso, C., and Molina, F. J. (1993). "Cover cracking as a function of bar corrosion: Part I—experimental test." *Mater. Struct.*, 26, 453–464.

Balafas, I. (2003). "Fibre-reinforced-polymers vs steel in concrete bridges: Structural design and economic viability." Ph.D. thesis, Engineering Dept. Univ. of Cambridge, Cambridge, UK.

Balafas, I., and Burgoyne, C. J. (2009). "Environmental conditions and corrosion initiation in concrete bridges." *Cem. Concr. Res.*, in press.

Balafas, I., and Burgoyne, C. J. (2010). "Environmental effects on cover cracking due to corrosion." *Cem. Concr. Res.*, 40(9), 1429–1440.

Bažant, Z. (1979a). "Physical model for steel corrosion in concrete sea structures—theory." *ACI Struct. J.*, 105(ST6), 1137–1153.

Bažant, Z. (1979b). "Physical model for steel corrosion in concrete sea structures—application." *ACI Struct. J.*, 105(ST6), 1155–1166.

Bhargava, K., Ghosh, A., Mori, Y., and Ramanujam, S. (2006). "Analytical model for time to cover cracking in RC structures due to rebar corrosion." *Nucl. Eng. Des.*, 236(11), 1123–1139.

Burgoyne, C. (2004). "Does FRP have an economic future?" *Proc. 4th Conf. on Advanced Composite Materials in Bridges and Structures, ACMBS4*, Calgary, Canada.

CEB. (1993). *Model code for concrete structures (MC-90)*, Thomas Telford, London.

González, J. A., Andrade, C., Alonso, C., and Feliu, S. (1995). "Comparison of rates of general corrosion and maximum pitting penetration on concrete embedded steel reinforcement." *Cem. Concr. Res.*, 25(2), 257–264.

Hutchinson, J. W., and Suo, Z. (1992). "Mixed mode cracking in layered materials." *Advances in applied mechanics*, Vol. 29, J. W. Hutchinson and T. Y. Wu, eds., Academic Press, San Diego, CA, 63–91.

Konopka, P. (2005). "Structural properties of rust." *4th-year undergraduate project*, Univ. of Cambridge, Cambridge, UK.

Liu, T., and Weyers, R. W. (1998a). "Modeling the dynamic corrosion process in chloride contaminated concrete structures." *Cem. Concr. Res.*, 28(3), 365–379.

Liu, T., and Weyers, R. W. (1998b). "Modeling the time-to-corrosion cracking in chloride contaminated concrete structures." *ACI Mater. J.*, 95(6), 675–681.

Liu, Y. (1996). "Modelling the time-to-corrosion-cracking of the cover concrete in chloride contaminated reinforced concrete structures." Ph.D. thesis, Virginia Polytechnic Institute and State Univ., Blacksburg, VA.

Maaddaay, T. E., and Soudki, K. (2007). "A model for prediction of time from corrosion initiation to corrosion cracking." *Cem. Concr. Compos.*, 29, 168–175.

Martin-Perez, B. (1999). "Service life modelling of RC highway structures exposed to chlorides." Ph.D. thesis, Univ. of Toronto, Toronto.

Martin-Perez, B., Zibara, H., Hooton, R. D., and Thomas, M. D. A. (2000). "A study of the effect of chloride binding on service life predictions." *Cem. Concr. Res.*, 30, 1215–1223.

Melchers, R. E. (2003a). "Mathematical modelling of the diffusion controlled phase in marine immersion corrosion of mild steel." *Corros. Sci.*, 45(5), 923–940.

Melchers, R. E. (2003b). "Modeling of marine immersion corrosion for mild and low-alloy steels—Part 1: Phenomenological model." *Corros. Sci.*, 59(4), 319–334.

Melchers, R. E., and Jeffrey, R. (2005). "Early corrosion of mild steel in seawater." *Corros. Sci.*, 47(7), 1678–1693.

Molina, F. J., Alonso, C., and Andrade, C. (1993). "Cover cracking as a function of bar corrosion: Part II—Numerical model." *Mater. Struct.*, 26, 532–548.

Nguyen, Q. T., Millard, A., Care, S., L'Hostis, V., and Berthaud, Y. (2006). "Fracture of concrete caused by the reinforcement corrosion products." *J. Phys. IV*, 136, 109–120.

Ohtsu, M., and Yosimura, S. (1997). "Analysis of crack propagation and crack initiation due to corrosion of reinforcement." *Constr. Building Mater.*, 11(7-8), 437–442.

Pantazopoulou, S. J., and Papoulia, K. D. (2001). "Modelling cover-cracking due to reinforcement corrosion in RC structures." *J. Eng. Mech.*, 127(4), 342–351.

Suda, K., Misra, S., and Motohashi, K. (1993). "Corrosion products of reinforcing bars embedded in concrete." *Corros. Sci.*, 35(5-8), 1543–1549.

Tepfers, R. (1979). "Cracking of concrete cover along anchored deformed reinforcing bars." *Mag. Concr. Res.*, 31(106), 3–12.

Timoshenko, S. (1956). *Strength of materials: Part II: Advanced theory and problems*, 3rd Ed., D. Van Nostrand Company, Princeton, NJ.

Torres-Acosta, A. A. (1999). "Cracking induced by localized corrosion of reinforcement in chloride contaminated concrete." Ph.D. thesis, College of Engineering, Dept. of Civil and Environmental Engineering, Univ. of South Florida, Tampa, FL.

Tuutti, K. (1980). "Service life of structures with regard to corrosion of embedded steel." *Performance of Concrete in Marine Environment, Third Int. Conf. Proc. (ACI SP-65)*, St. Andrews-by-the-Sea, Canada, 223–236.

Uomoto, T., and Mirsa, S. (1988). "Behavior of concrete beams and columns in marine environment when corrosion of reinforcing bars takes place." *Concrete in the Marine Environment: Proc. of the 2nd Int. Conf., SP-109*, V. M. Malhotra, ed., 127–146.

Wang, X. H., and Liu, X. L. (2004). "Modelling effects of corrosion on cover cracking and bond in reinforced concrete." *Mag. Concr. Res.*, 56(4), 191–199.

Wegner, W., and Yaggi, M. (2001). "Environmental impacts of road salt and alternatives in the New York City watershed." *Stormwater*, 2(5).

Weyers, R. E. (1998). "Service life model for concrete structures in chloride laden environments." *ACI Mater. J.*, 95(4), 445–453.

Williamson, S. J., and Clark, L. A. (2000). "Pressure required to cause cover cracking of concrete due to reinforcement corrosion." *Mag. Concr. Res.*, 52(6), 455–467.

Zhao, Y. X. (2006). "Modeling the amount of steel corrosion at the cracking of cover concrete." *Adv. Struct. Eng.*, 9(5), 687–696.